Schreurs, G., Hänni, R & Vock, P. 2002. The influence of brittle-viscous multilayers on faulting during rifting: an analogue modelling approach. In: Schellart, W. P. and Passchier, C. W. 2002. Analogue modelling of large-scale tectonic processes. Journal of the Virtual Explorer, 7, 89-96.

The influence of brittle-viscous multilayers on faulting during rifting: an analogue modelling approach

G. SCHREURS[1], R. HÄNNI[1] & P. VOCK[2]

[1] *Institute of Geological Sciences, University of Bern, Baltzerstrasse 1, CH-3012 Bern, Switzerland*
email: schreurs@geo.unibe.ch
[2] *Institute of Diagnostic Radiology, Inselspital, CH-3010 Bern*

Abstract: Analogue model experiments were done to study the influence of brittle-viscous multilayers on faulting during rifting. In each experiment a lower viscous layer was placed over the entire base of the model, whereas a second interbedded viscous layer separated lower brittle strata from upper brittle strata. The presence of an interbedded viscous layer led to the development of two independent, decoupled conjugate normal fault systems in upper and lower brittle strata. Initial width between conjugate faults depended on the thickness of the brittle strata overlying a viscous layer. With progressive extension, fault-bounded blocks rotated about horizontal axes. Rotations of these fault blocks and accompanied lateral viscous flow caused locally reverse faulting in upper brittle strata. Continued extension eventually led to local linkage between faults in lower and upper brittle strata. Location and orientation of extensional transfer zones were directly linked to the geometry of the interbedded viscous layer. Where the initial boundaries of the upper viscous layer were parallel to the extension direction, the strike of the transfer zones was also parallel. Where this boundary was oblique, the strike of the transfer zones was also oblique.

Introduction

Rift systems and divergent continental margins are the result from extension of the continental lithosphere. Understanding the physical parameters that control the development and evolution of faults in rifts and divergent margins is important for their interpretation in nature and for assessing their spatial distribution (e.g., orientation and spacing) and temporal evolution. Structures such as those interpreted from seismic sections across the North Sea graben suggest that thickness and distribution of weak layers (such as salt) and pre-rift faults have played a major role on the subsequent development of graben structures (Stewart et al., 1996; Stewart, 1999). Other factors that are considered to influence the geometry and evolution of rifts include the orientation of the regional stress field (i.e. extension vs. oblique extension), synkinematic sedimentation and strain rate (salt has a time-dependent rheological behaviour).

Extensional analogue models to date have largely been of two kinds: (i) those where a deformable hanging-wall block is translated over a rigid, non-deformable footwall, and (ii) those that involve extension above a basement that undergoes a stretching deformation. Although the first type of model has yielded valuable information on specific extension-related structures, such as roll-over anticlines in the hangingwall of listric normal faults (e.g., McClay et al., 1991), the fact that the footwall is not allowed to undergo deformation is a limitation for modelling rifts and passive margins. Extension experiments of sandpacks above a stretching basement by McClay & Ellis (1987) showed that the geometries of both faults and fault blocks change with progressive deformation, and that extension above a sloping basement resulted in faults dipping in the same direction as the detachment.

We carried out experiments to investigate the influence of brittle-viscous multilayers on faulting in models undergoing a stretching deformation. Models were analysed by X-ray computerised tomography (Hounsfield, 1973) a non-destructive technique that allows a detailed study of the internal geometry and kinematics of analogue models.

Analogue materials and experimental procedure

In normal gravity experiments dry granular materials with low cohesion are commonly considered to be a good analogue for brittle rocks in the upper crust, because they obey the Mohr-Coulomb criterion of failure. Viscous materials on the other hand, are generally used to simulate viscous flow of salt or evaporites in the upper crust or rocks in the lower crust. We selected quartz sand (grain size: 80-200 μm) and corundum sand (grain size: 90-125 μm) as brittle analogue materials. The angles of internal friction for quartz and corundum sand are 35° and 36°, respectively, and these materials can be used to simulate upper crustal rocks which have comparable angles of internal friction at low normal stresses (Byerlee, 1978). We used a Newtonian viscous polymer (polydimethylsiloxane, PDMS) as viscous analogue material. This transparent material has a linear viscosity of 5 x 10^4 Pa.s at room temperatures and at strain rates below 3 x 10^{-3} s^{-1} (Weijermars, 1986).

The experimental apparatus comprised a rectangular box, whose wooden base was overlain by an alternation of nine plexiglass bars (each bar is 5 mm wide, 5 cm high and 80 cm long) and eight foam bars (each bar is 3 cm wide, 5 cm high and 80 cm long). Before constructing the stratified brittle-viscous analogue model, the assemblage

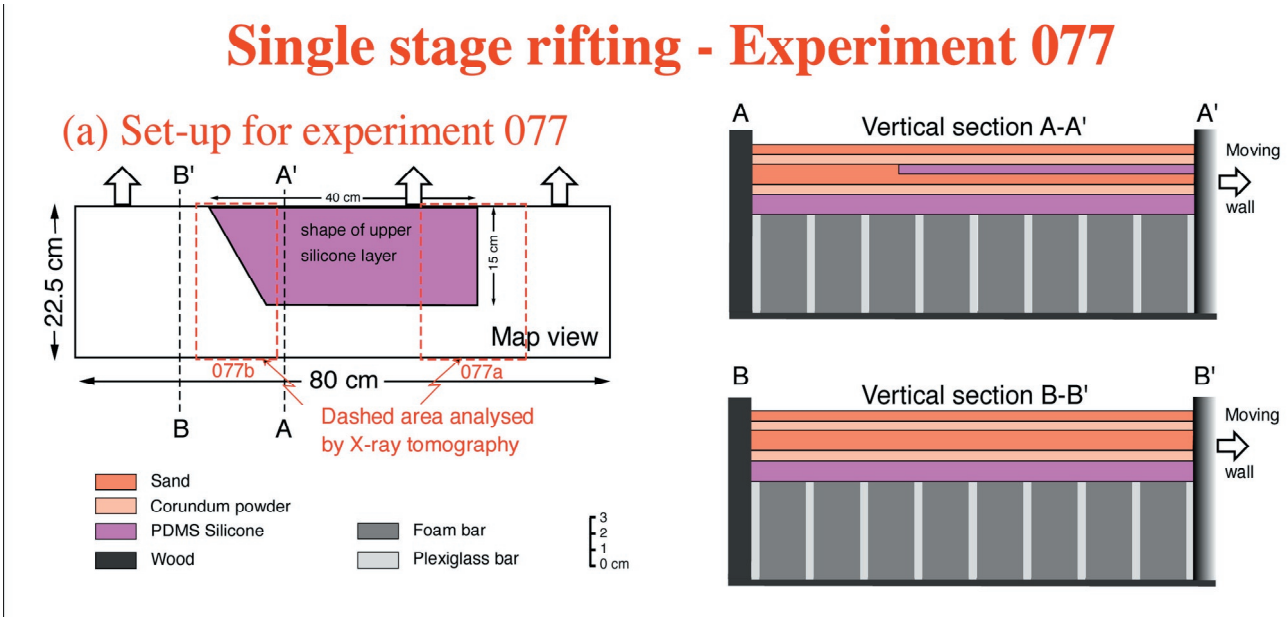

Figure 1. Experimental set-up for single stage rifting experiment 077 schematically illustrated by a plan view and two vertical sections. Two areas (077a and 077b) were analysed by X-ray tomography. Initial grid spacing on surface was 4 cm; grid consisted of coloured sand.

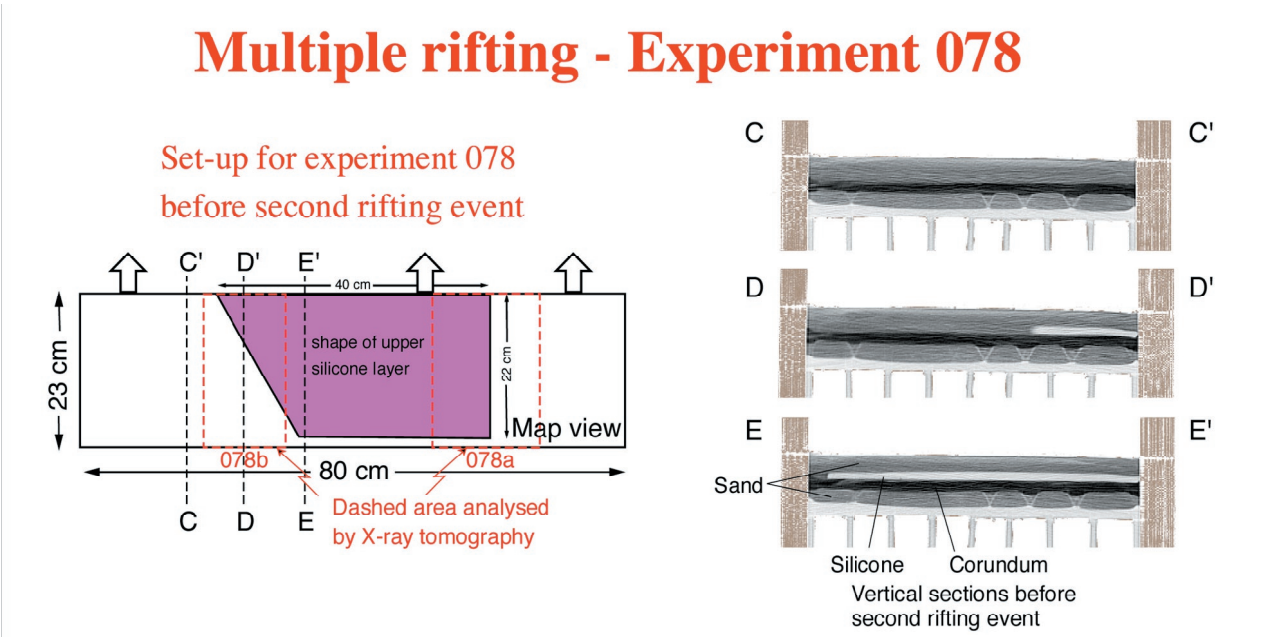

Figure 2. Plan view and vertical sections depict the set-up for multiple rifting experiment 078 before the onset of the second rifting event. Two domains (078a and 078b) were analysed by X-ray tomography. Initial grid spacing on surface was 4 cm.

of plexiglass and foam bars was shortened 6 cm by displacement of a mobile vertical wall. In the shortened state, the width of each foam bar was reduced to ca. 2.25 cm, whereas the width of the plexiglass bars remained unchanged. The brittle-viscous multilayer model was then constructed on top of the shortened assemblage. A 1 cm thick layer of viscous PDMS was placed directly over the assemblage of plexiglass and foam bars. The stratified model was completed by adding brittle and viscous layers. The presence of foam bars alternating with plexiglass bars in combination with the overlying basal viscous layer prevented localisation of deformation near the extending mobile wall. The foam bars "decompressed" during extension and deformation was distributed over the width of the model. Displacement of the vertical mobile wall, driven by a motor, produced extension of the model at a constant velocity of 2.4 cm/h

Experiment 077 simulated single stage rifting. The length of the brittle-viscous model was 80 cm, and the initial width was 22.5 cm. The undeformed multilayered model consisted of a 1 cm thick basal viscous layer (PDMS) and an upper, 5 mm thick viscous layer embedded in brittle strata made up of corundum and quartz sand (Fig. 1). Total initial height of the model was 3.5 cm. The upper viscous layer was placed adjacent to the extending mobile wall. It had one PDMS-sand boundary parallel to the extension direction, and the opposite boundary oblique to the extension direction (at an angle of 30°). The width of

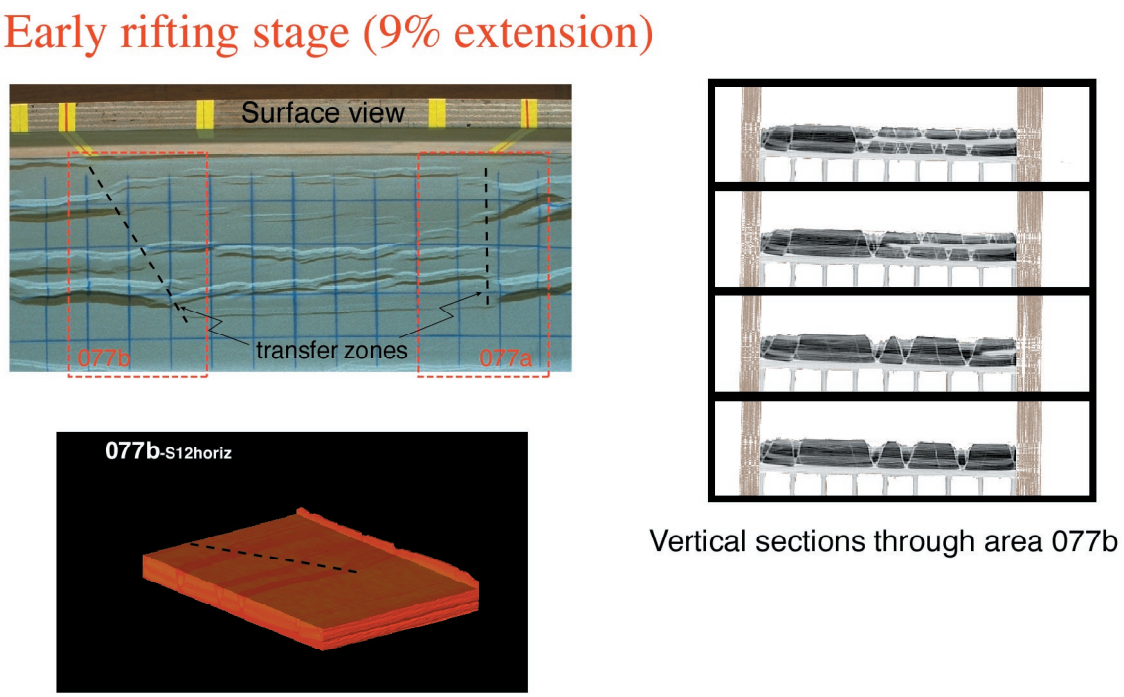

Figure 3. Structures in experiment 077 after 9% extension as seen in surface view, vertical sections and in cut-out view. Black dashed lines in surface view indicate major transfer zones located above the interbedded viscous layer. Dashed red rectangles indicate areas analysed by X-ray tomography.

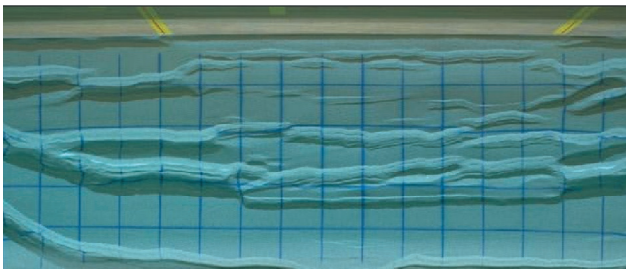

Figure 4 (right). Movie showing surface evolution of experiment 077. Note the difference in graben width between domain with a second, interbedded viscous layer (see Fig. 1 for its location) and adjacent domains with only a basal viscous layer. Initial grid spacing on surface was 4 cm. First frame is after 5 mm of extension. Subsequent frames are at 5 mm extension increments. (**Select image for movie**)

the upper viscous layer was 15 cm, and the length of the layer near the mobile wall was 40 cm. Total extension of the model amounted to 5 cm or 22.2%.

In the multiple rifting experiment 078 (Fig. 2), the initially stratified model consisted of a 1 cm thick basal viscous layer, overlain by 1 cm sand. The length of the model was 80 cm and the initial width was 20.5 cm. During the first stage of rifting the model was extended by 2.5 cm or 12.2%. Conjugate normal faults formed in the brittle sand layers and extended down to the top of the viscous layer (Fig. 2). The experiment was temporarily halted and the grabens were filled with corundum powder. An additional 5 mm thick layer of corundum was sprinkled on top. A 5 mm thick viscous PDMS layer was now placed on top covering part of the corundum layer, and the PDMS layer itself was overlain by 10 mm of sand. The width of the PDMS layer was 22 cm and it was placed right adjacent to the extending mobile wall.

Its shape was very similar to the upper viscous layer in experiment 077. It had one PDMS-sand boundary parallel to the extension direction, and the opposite boundary at an angle of 30° to the extension direction. The second stage of rifting consisted of an additional 5 cm extension. Final width of the model was 28 cm and total extension (with respect to undeformed stage) was 36.6%.

Deformation of the analogue model took place in the investigation field of a helical X-ray computerized tomographer, and 3-D volumetric raw data were acquired of two parts of the model (see Fig. 1 and 2) at the initial undeformed state and after every 5 mm of progressive extension. The 3-D raw data allowed the computation of contiguous cross-sectional slices perpendicular to the long dimension of the model, i.e. parallel to the extension direction. Computer visualisation software was used to reconstruct the analogue model in three dimensions and to reconstruct horizontal and longitudinal sections. On the basis of 3-D reconstructions, computer animations were created in order to study the spatial evolution of structures at a specific stage, or to study the 4-D evolution (i.e. 3-D evolution with time) of the model.

Experimental results

Single stage rifting - Experiment 77

The evolution of the fault pattern in the single stage rifting experiment as seen in surface view (Fig. 3 & 4) is closely related to the distribution of brittle and viscous layers at depth. In domain with a basal viscous layer overlain by brittle layers, the spacing between conjugate normal faults was larger than in the domain that had a second, upper

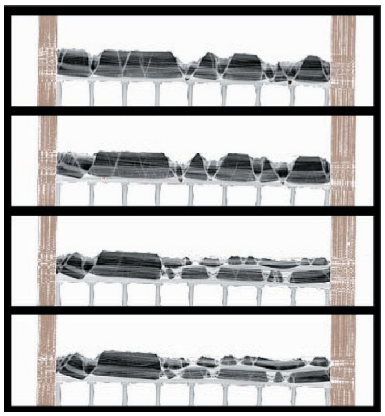

Figure 5. Successive vertical CT images through the brittle-viscous model (domain 077a; see Fig. 3): two sections cross the domain with two viscous layers (upper two images), and two the domain with only a basal viscous layer overlain by brittle layers (lower two images). Corundum is dark grey; sand is medium-grey, and viscous PDMS is light-grey. Initial width of model was 22.5 cm and initial height 3.5 cm. Extension increment between frames is 5 mm. (**Select image for movie**)

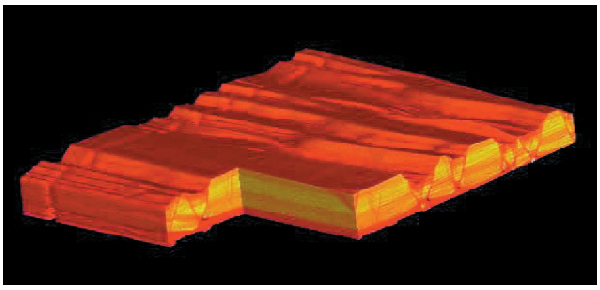

Figure 6. Movie of 3D evolution with time of experiment 077 (domain 077a; see Fig. 3) showing the development of a transfer zone parallel to the extension direction. Each frame shows a cut-out 3D view that consists of 80 serial cross sections each representing a 2 mm thick CT slice. Extension increment between frames is 1 cm. Viscous silicone (PDMS) is red, quartz sand is orange and corundum powder is a dark yellow to orange. (**Select image for movie**)

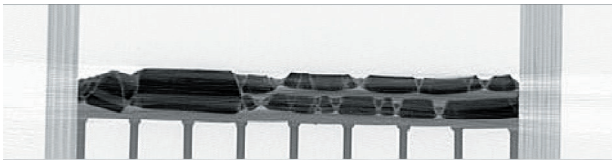

Figure 7 (left). Movie showing the geometry of part of experiment 077 by 80 serial vertical sections after 9% extension. Note the drastic change in structural style as soon as the interbedded viscous layer appears. (**Select image for movie**)

viscous layer embedded in brittle layers (see experimental set-up; Fig. 1). As normal faults propagated along strike they either linked or overlapped with other sub-parallel oriented faults. In some cases lateral propagation of different normal fault segments induced a change in fault orientation in the area where they met. With progressive extension, new faults appeared within previously formed grabens. Extensional transfer zones mark the transition between widely spaced conjugate faults and narrowly spaced conjugate faults and closely mimic the position of the underlying interbedded weak layer. Where this boundary is initially parallel to the extensional direction, the alignment of transfer zones is also more or less parallel to it; where this border is initially at an angle of 30° to the extension direction, the transfer zones also forms at an angle of 30°. Note that normal faults in the domain above the interbedded weak layer did not form instantaneously across the entire long dimension of this domain. As a result some transfer zones also formed in this domain.

Fig. 5 shows the evolution of structures in four cross-sections through part of the model. The fault evolution was very different in domains with and without an interbedded viscous layer. In those parts of the model with an interbedded weak layer progressive extension resulted in decoupled conjugate normal fault systems in upper and lower brittle strata. The horizontal distance between graben-bounding normal faults was small and the offset along individual faults was limited. In contrast, in the domain without a second interbedded viscous layer, the grabens were fewer, deeper and wider, and faults extended all the way down to the top of the basal viscous layer. Initial graben width reflects the depth to the viscous layer. A larger vertical distance to the viscous layer results in a wider graben. Fault offset along existing faults increased with progressive extension. In large grabens new steep normal faults formed that are antithetic to the bounding faults and merged with them at depth. Although normal faults at early stages of extension were straight in cross-section, they became listric with progressive deformation and fault-bounded blocks rotated about a horizontal axis. In the domain with an interbedded viscous layer, conjugate normal fault systems in the lower brittle compartment formed at different locations than in the upper brittle compartment. The formation of conjugate normal faults in the lower compartment caused a downbending of the overlying brittle compartment and lateral flow of the interbedded viscous layer. At the final stages of extension, parts of the upper brittle compartment were in contact with the lower brittle compartment.

Fig. 6 shows the 3D evolution of part of the model with time. Progressive extension manifested itself differently in domains with and without an interbedded viscous layer. In the latter domain grabens are fewer, wider and deeper. Transfer zones form in the transition zone between the two domains. Fig. 7 illustrates the drastic lateral changes in the structural style across the transition zone by 80 serial vertical cross-sections at 9% extension. Oblique transfer zones that strike parallel to the boundary of the interbedded viscous layer (Fig. 8) can be followed at depth in Figs. 8 and Fig. 9. The latter figure consists of a series of horizontal sections at 9% extension. Fig. 10 shows the structures in experiment 077 at 18% extension, while

Experiment 077 - 9% extension

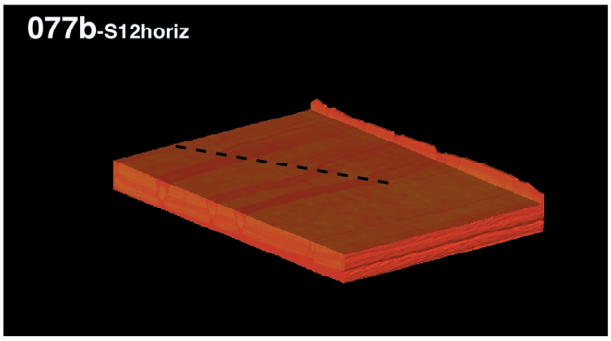

Figure 8. Horizontal section through 3D cut-out perspective view showing oblique transfer zone after 9% extension (domain 077a; cf. Fig. 3).

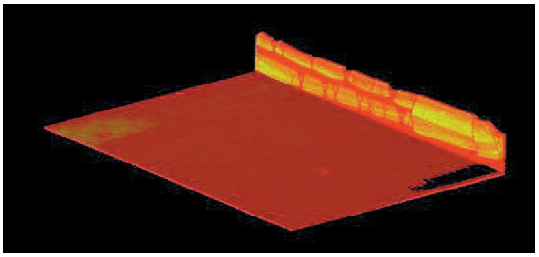

Figure 9. Successive horizontal sections through 3-D perspective view after 9% extension (domain 077b). The location of the oblique extensional transfer zone is linked to the oblique boundary of the interbedded viscous layer. (**Select image for movie**)

Experiment 077 -18% extension

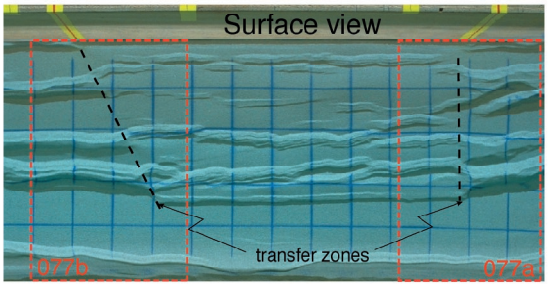

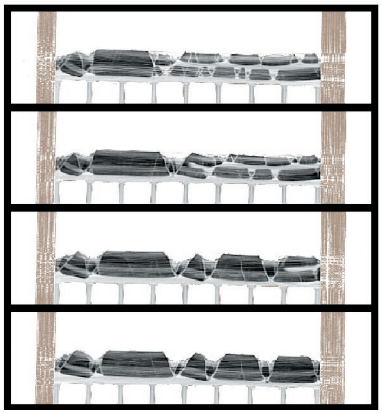

Vertical sections through area 077b

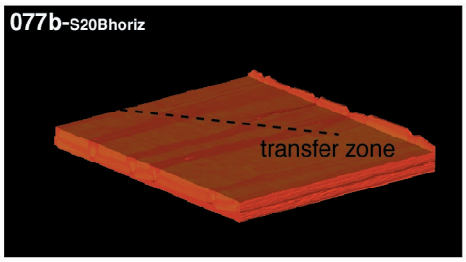

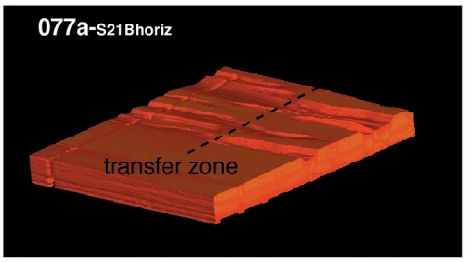

Figure 10. Structures in experiment 77 after 18% extension illustrated by surface photograph, vertical sections and two cut-out 3-D perspective views. Transfer zones are related to the shape and position of the interbedded viscous layer. (**Select image for movie**)

Fig. 11 and 12 show serial horizontal sections through transfer zones at the same stage of deformation. Note how some of the faults in the lower brittle compartment – below the interbedded viscous layer - die out laterally towards the domain with only one basal viscous layer.

Multiple rifting - Experiment 78

In experiment 078 the model underwent two stages of rifting. Extension during the first rift event amounted to a little over 12% and resulted in the development of conjugate normal fault systems in the brittle layer (Fig. 2). Grabens were filled with granular material and overlain by additional brittle and viscous material (Fig. 2). Subsequently the model underwent a second rifting event with the same direction of extension. Fig. 13 shows the surface evolution after 6.5% extension during the second rifting event, while the evolution of structures in four cross-sections is shown in Fig. 14. The first frame in Fig. 14 shows the conjugate normal faults that formed during the first rifting event. Extension during the second rifting event caused immediate reactivation of the pre-existing normal faults. In the brittle-viscous domain with only one viscous layer, faults propagated toward the surface. In the domain with two viscous layers, however, faults only propagated upward as far as the interbedded viscous layer. New faults formed in the upper brittle compartment, but sideways displaced with respect to faults in the lower brittle compartment. Grabens in the upper brittle compartment formed in those areas where horsts formed in the lower brittle compartment. Faults acquired a listric shape with progressive extension and fault-bounded blocks underwent rotations about a horizontal axis. Block

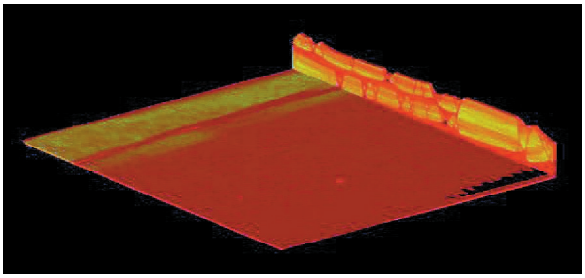

Figure 11. Successive horizontal sections through 3-D perspective view after 18% extension (domain 077b; see Fig. 10). (**Select image for movie**)

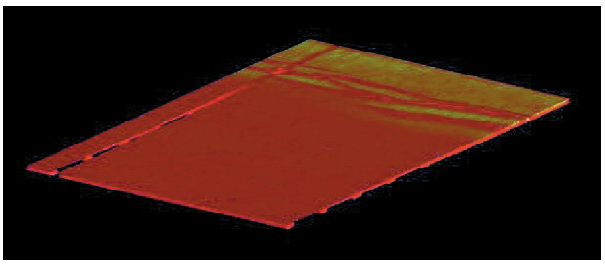

Figure 12. Successive horizontal sections through 3-D perspective view after 18% extension (domain 077a; see Fig. 10). (**Select image for movie**)

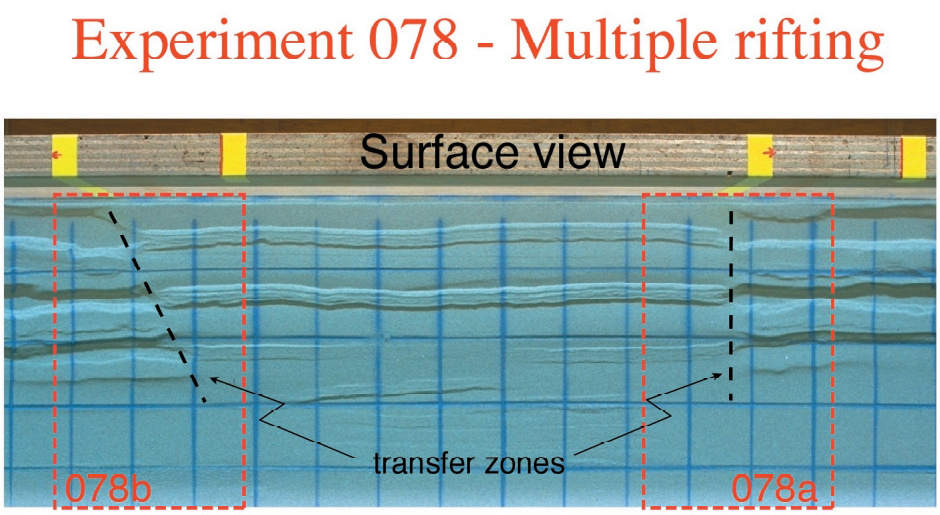

Figure 13. Surface photograph of experiment 078 after 6.5% extension during the second rifting event. Black dashed lines indicate major transfer zones located above the interbedded viscous layer. Dashed red rectangles indicates areas analysed by X-ray tomography.

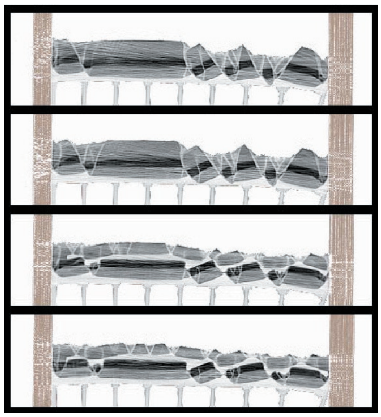

Figure 14. Successive vertical CT images through experiment 078 (domain 078a, see Fig. 13): two sections cross the domain with only a basal viscous layer overlain by brittle layers (upper two images), and two sections the domain with two viscous layers (lower two images). Corundum is dark grey; sand is medium-grey, and viscous PDMS is light-grey. After the first rifting event the width of model was 23 cm and the height was 3.5 cm. Extension increment between frames is 5 mm. (**Select image for movie**)

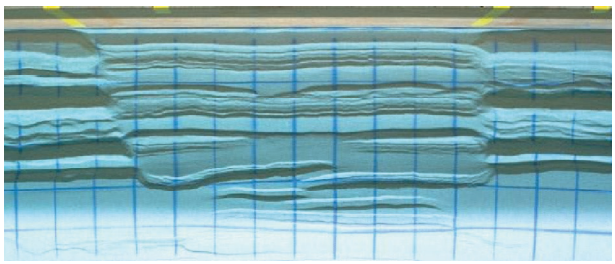

Figure 15. Movie showing surface evolution of experiment 078. Note the difference in graben width between domain with interbedded viscous layer (cf. Fig. 2 for its location) and adjacent domains. Initial grid spacing on surface was4 cm. Extension increment between frames is 5 mm. (**Select image for movie**).

rotations in the lower brittle department influenced as yet unfaulted domains in the upper brittle compartment and locally created new, strongly curved faults in the upper brittle compartment along which small fault blocks are squeezed upward. These curved faults have a dip-slip component at its lower end and a reverse-slip component at the surface.

Figure 15 shows the progressive evolution of structures in surface view and illustrates the distinct fault pattern between the domain underlain by one viscous layer (large grabens) and the domain underlain by two viscous layers (smaller grabens). In the former domain the location of the grabens is controlled by the faults that formed during the first rifting event, and the initial width of the grabens

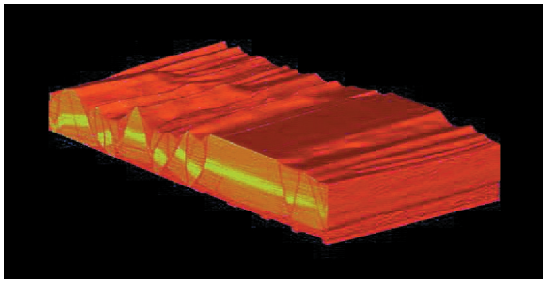

Figure 16 (left). Movie of 3D evolution with time of experiment 078 (domain 078b, cf. Fig. 13) showing the development of a transfer zone oblique to the extension direction. Each frame shows a cut-out 3D view that consists of 80 serial cross sections each representing a 2 mm thick CT slice. Extension increment between frames is 1 cm.
(**Select image for movie**)

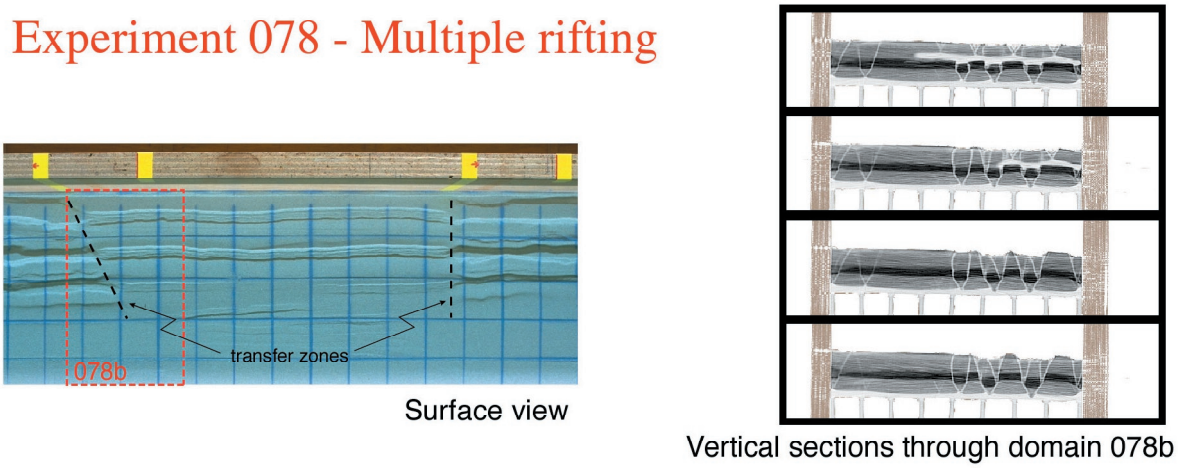

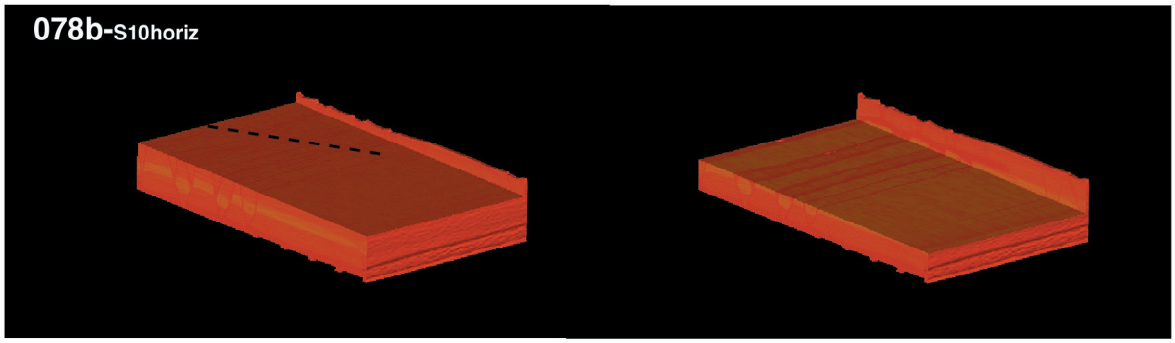

Figure 17. Structures in experiment 078 after 6.5% extension during second rifting event, illustrated by surface photograph, vertical sections and two cut-out 3-D perspective views. Transfer zones are related to the shape and position of the interbedded viscous layer.

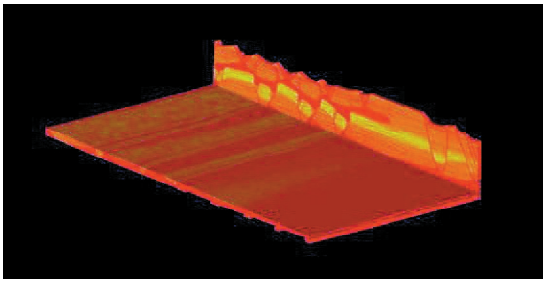

Figure 18. Horizontal sections through 3D cut-out perspective view showing oblique transfer zone after 6.5% extension during the second rifting event (domain 078b; see. Fig. 17). (**Select image for movie**)

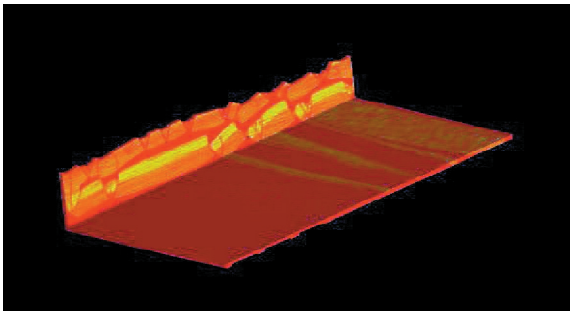

Figure 19. Successive horizontal sections through 3-D perspective view at 6.5% extension during the second rifting event (domain 078b; see Fig. 17). The location of the oblique extensional transfer zone is linked to the oblique boundary of the interbedded viscous layer. (**Select for movie).**

is determined by the depth to the basal viscous layer. In the latter domain, however, the interbedded viscous layer did not allow the reactivated normal faults in the lower brittle compartment to reach the surface. Fig 16 shows the 3D progressive evolution of part of experiment 078. As in the previous experiment, the location and orientation of extensional transfer zones is related to the shape of the interbedded viscous layer (Fig. 17). However, in contrast to experiment 77 the normal faults in the lower brittle compartment do not die out along strike, but continue into the domain with only a basal viscous layer. Consequently, sections through the lower brittle compartment do not show a transfer zone (Fig. 18 & 19). Figs. 20 and 21 show the structures in experiment 078 at a more advanced stage of multiple rifting (after 15% extension during the second rifting event).

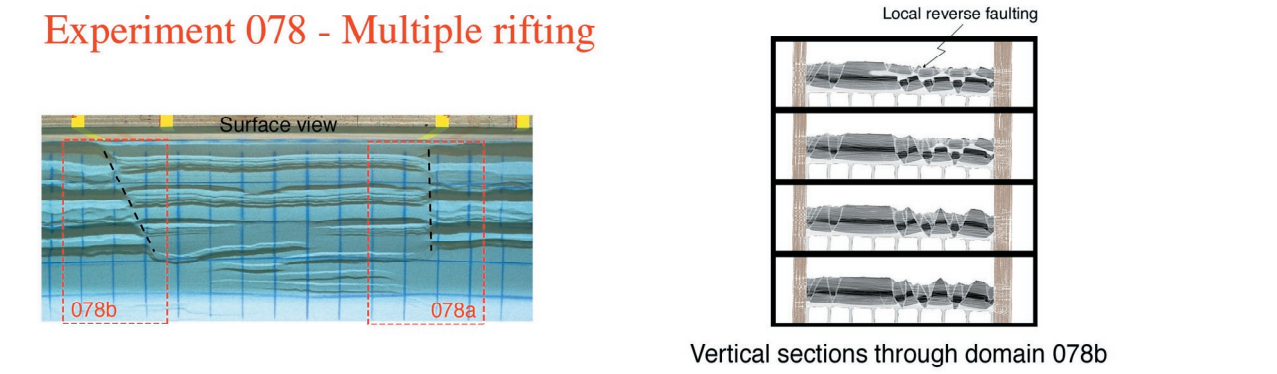

Figure 20. Structures in experiment 078 after 15% extension during second rifting event, illustrated by surface photograph, vertical sections and three cut-out 3-D perspective views.

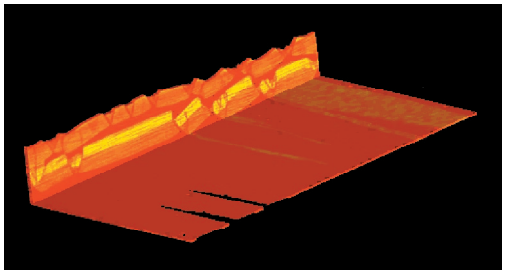

Figure 21 (right). Successive horizontal sections through 3-D perspective view at 15% extension during second rifting event (domain 078a; see Fig. 17). Note the absence of a transfer zone in the lowermost part of the model. **(Select image for movie)**

Concluding remarks

The shape and position of the upper viscous layer had a profound influence on the structural style that developed in the course of the experiment. The upper viscous layer embedded within brittle strata initially caused the development of two independent, decoupled conjugate normal fault systems in upper and lower brittle compartments. The width between conjugate normal faults is related to the depth to the viscous layer. In the part of the model where there was only one basal viscous layer overlain by brittle materials, the width between conjugate faults was large, whereas in that part of the model with a second, upper viscous layer embedded in brittle layers, this width was smaller. In the multiple rifting experiment, the faults that formed during the first rifting event were reactivated and controlled the fault pattern in the overlying brittle layers. The interbedded viscous layer, however, halted upward fault propagation. Conjugate normal faults formed in the upper brittle compartment that were decoupled from the reactivated normal faults in the lower brittle compartment. The location and orientation of extensional transfer zones, visible in horizontal sections and in surface view, was directly linked to the geometry of the interbedded viscous layer. In case the boundary between the interbedded viscous layer and adjacent brittle layers was oblique to the extension direction, vertical transfer zones also formed oblique. In case this boundary was parallel to the extension direction, the transfer zones were also parallel. The experiments suggest that the width between conjugate fault systems and the position and orientation of extensional transfer zones in nature might be directly linked to initial lateral rheological changes within a layered sequence.

Acknowledgments

Research was funded by the Hochschulstiftung Bern and a grant from the Swiss National Science Foundation (Nr. 2000-055411.98/1).

References

Byerlee, J.D., 1978. Friction of rocks. Pure Applied Geophysics, 116, 615-626.

Hounsfield, G.N., 1973, Computerized transverse axial scanning (tomography). British Journal of Radiology, 46, 1016-1022.

McClay, K.R. & Ellis, P.g., 1987. Geometries of extensional fault systems in model experiments. Geology, 15, 341-344.

McClay, K.R., Waltham, D.A., Scott, A.D. & Abousetta, A., 1991. Physical and seismic modelling of listric normal fault geometries. Geological Society Special Publication, 56, 231-239.

Stewart, S.A., Harvey, M.J., Otto, S.C. & Weston, P.J., 1996. Influence of salt on fault geometry. Examples from the UK salt basins. In: Alsop, G.I., Blundell, D.J. & Davison, I. (Eds.). Salt Tectonics. Geological Society Special Publication, 100, 175-202.

Stewart, S.A., 1999. Geometry of thin-skinned tectonic systems in relation to detachment layer thickness in sedimentary basins. Tectonics, 18, 719-732.

Weijermars, R., 1986. Flow behaviour and physical chemistry of bouncing putties and related polymers in view of tectonic laboratory applications. Tectonophysics, 124, 325-358.